Results in Optics 5 (2021) 100111

Contents lists available at ScienceDirect

Results in Optics

journal homepage: www.sciencedirect.com/journal/results-in-optics

Reflective coupled microring resonators for reconfigurable photonic systems: Performance analysis

Fekadu Mihret Geremew *, Talabattula Srinivas

Indian Institute of Science, Applied Photonics Lab, Department of Electrical Communication Engineering, CV Raman Road, Bangalore 560012, India

ARTICLE INFO

Keywords:
Beamforming
Filters
Microring resonators
Photonics
Optical logical operation
Optical true time delay

ABSTRACT

We propose reflective type triple coupled microring resonators (TCMMRs) for reconfigurable photonic based systems. We have developed an analytical model and analyzed its useful performance characteristics. The TCMMRs based device exhibits a wide range of performance characteristics such as multi-band filtering, optical logical operations, and optical true-time delay lines. Reconfigurable multiple resonances and their splitting features associated with the device provide useful filtering performance characteristics such as high out-of-band rejection, flat-top bandwidth, and near to ideal shape factor. The device can perform multiple functions such as bandpass, bandstop, and notch filtering with a good performance. Unlike two input narrowband logical operations demonstrated in the literature, our proposed device can perform as three-input optical logical operator, and it can switch wideband microwave frequency signals optically. Moreover, the device exhibits wideband flat top group delay response. It carries out delay tuning using a single variable coupling coefficient which simplifies the complexity of the tuning encountered in binary tree-structured optical beamforming networks based on conventional microring resonators.

1. Introduction

Optical Microring resonators (MRRs) have been playing profound roles in a multitude of application areas such as communication and information processing (Zhang et al., 2008; Toumasis et al., 2021; Zhang, et al., 2008), optical and biomedical sensing (Yao et al., 2018; Zhu et al., 2017), electro-optic modulation (Sun et al., 2019; Mohammadi et al., 2012), microwave photonic signal processing (Wu et al., 2016; Capmany and Novak, 2007) and so on. The most attractive features of MMRs are their high efficiency and flexibility in the manipulation of light within confined small footprint and suitability for integrated photonics.

Even though MRR is efficient in manipulating light, it has a drawback of producing narrowband Lorentzian magnitude and group delay responses with very sharp peaks or notches, resulting in distortion of signal processing. Thus, researchers have proposed many ways to increase operational bandwidth and avoid signal distortion. For instance, to get a sizeable flat-top bandwidth, a very high order of eleven serially coupled microring resonators based on bandpass filters (Little, 2004) are proposed for WDM applications with the performance of 50 GHz and 25 GHz bandwidth and out-of-band rejection ratio exceeding 80 dB. Additionally, bandpass filters based on cascading of second stage microring resonators, in (Hu et al., 2012), have been demonstrated with the out-of-band rejection of 44.0 dB and 3 dB bandwidths of 16.61 GHz when five stages are cascaded. In (Geremew and Talabattula, 2021), a reconfigurable multifunctional photonic filter that can function as a flat-top wideband bandpass filter, bandstop, and notch filter has been proposed, and its performance has been analyzed.

Moreover, continuously tunable true-time delay performance has been demonstrated by cascading many ring resonators (Cardenas et al., 2010; Xie et al., 2014) to increase bandwidth and time delay. Finally, bandpass and bandstop responses at a single port cannot be achieved in conventional MRRS. This problem is solved using an additional degree of freedom that utilizes reflection (Huang et al., 2018, 2019).

In this paper, we have introduced a device based on three mutually coupled MRRs. This device structure was first introduced by Otto Schwelb as band limited optical mirror (Schwelb, Nov. 2005). The performance, as a reflective mirror, was analyzed numerically using scattering matrix formulation. To the best of our knowledge, the device's feasibility study for reconfigurable photonic systems has not been conducted, and its analytical model has not been developed so far in the literature. Therefore, We have developed an analytical model and

* Corresponding author.
E-mail address: fekadug@iisc.ac.in (F.M. Geremew).

https://doi.org/10.1016/j.rio.2021.100111
Received 10 March 2021; Received in revised form 15 May 2021; Accepted 13 June 2021
Available online 19 June 2021

analyzed its performance for the filtering applications, the optical logical operation in microwave applications, and the optical true-time delay line in optical microwave beamforming applications.

2. Mathematical modelling of TCMRRS

The proposed device based on the triple coupled microring resonator is shown in Fig. 1(a). The three microrings R1, R2, and R3 couple mutually at coupling regions 2, 3, 4, and joining their centres form an equilateral triangle. The first microring R1 couples to a waveguide at coupling region 1. The length of the microrings is assumed to be L, and their portions bounded by the coupling regions 2,3, and 4 have the length L/6. These curves form arcs of 60 degrees (i.e., 60/360*L = L/6). The electric field with A_1^+ is incident to the straight waveguide at coupling region 1. Part of it is transmitted as B_1^+, and another is coupled to R1 as b_1^+. We can observe that two contra propagating modes exist on each microring when we trace the coupling of fields and the corresponding propagations on each microring resonator. The anticlockwise propagating fields are designated by the '+' sign, and clockwise propagating fields are designated by '-'sign. Because of contra propagating modes in each microring resonator, there is the reflected field A_1^- which propagates opposite to the incident field A_1^+. The electric field amplitudes in each microring resonators are controlled by self and cross coupling coefficients (t_1,k_1), (t_2,k_2),(t_3,k_3) and (t_4,k_4).

Device reconfigurability can be done using thermal tuning as shown in Fig. 1(b) which is suitably adopted structure for layout design and fabrication. We have to note that the shape of the microrings doesn't affect the performance whether it is circular or rectangular as far as it is a closed path. For the specified technological platform, for example SOI, the performance determinant factors are the length of ORR and its coupling strength with other waveguides. The mode overlap loss of straight and curved section is negligible for a bending radius greater than 10 μm for SOI platform. Mach Zehnder interferometers (MZIs) are inserted in the coupling sections of three mutually coupled MRRs.

To be consistent with the original circular coupled microrings from which our analytical equations have been derived, We have to keep the lengths of the common regions to be one-sixth of the total length of individual ORRs or L/6 units, and the other part of each microring should be 5L/6 units, where L is the length of the microrings. Since there are multiple vertical and horizontal straight waveguide sections, it is easy to control the Length L of each microring to be identical. The MZI with 3 dB directional coupler is used for tuning coupling coefficients ti and ki. Thermal heaters can be placed 1um to 2 um above one of MZI arms. The self and cross coupling amplitude coefficients of MZI with 3 dB coupler are tuned as $k_i = 0.5\cos(\phi_i/2), t_i = 0.5\sin(\phi_i/2)$, i = 1,2, …,4. The phase induced ϕ_i in the i^{th} MZI is $\phi_i = \Delta n T_{ti} L/\lambda$, where Δn is thermally induced refractive index constant of waveguides, T_{ti} is the temperature in kelvin induced in the i^{th} MZI arm, L is the length of MZI arm, λ is operation wavelength.

Using the transfer matrix analysis technique (Poon et al., 2004; Li et al., 2013), the optical field relations on the coupling regions are expressed as

$$\begin{pmatrix} B_1^+ \\ b_1^+ \end{pmatrix} = \begin{pmatrix} t_1 & -jk_1 \\ -jk_1 & t_1 \end{pmatrix} \begin{pmatrix} A_1^+ \\ a_1^+ \end{pmatrix}; \begin{pmatrix} A_1^- \\ b_1^- \end{pmatrix} = \begin{pmatrix} t_1 & -jk_1 \\ -jk_1 & t_1 \end{pmatrix} \begin{pmatrix} B_1^- \\ a_1^- \end{pmatrix} \quad (1)$$

$$\begin{pmatrix} d_1^+ \\ b_2^- \end{pmatrix} = \begin{pmatrix} t_2 & -jk_2 \\ -jk_2 & t_2 \end{pmatrix} \begin{pmatrix} c_1^+ \\ a_2^- \end{pmatrix}; \begin{pmatrix} f_1^- \\ a_2^+ \end{pmatrix} = \begin{pmatrix} t_2 & -jk_2 \\ -jk_2 & t_2 \end{pmatrix} \begin{pmatrix} e_1^- \\ d_2^+ \end{pmatrix} \quad (2)$$

$$\begin{pmatrix} d_3^+ \\ d_2^- \end{pmatrix} = \begin{pmatrix} t_3 & -jk_3 \\ -jk_3 & t_3 \end{pmatrix} \begin{pmatrix} c_3^+ \\ c_2^- \end{pmatrix}; \begin{pmatrix} b_3^- \\ c_2^+ \end{pmatrix} = \begin{pmatrix} t_3 & -jk_3 \\ -jk_3 & t_3 \end{pmatrix} \begin{pmatrix} a_3^- \\ b_2^+ \end{pmatrix} \quad (3)$$

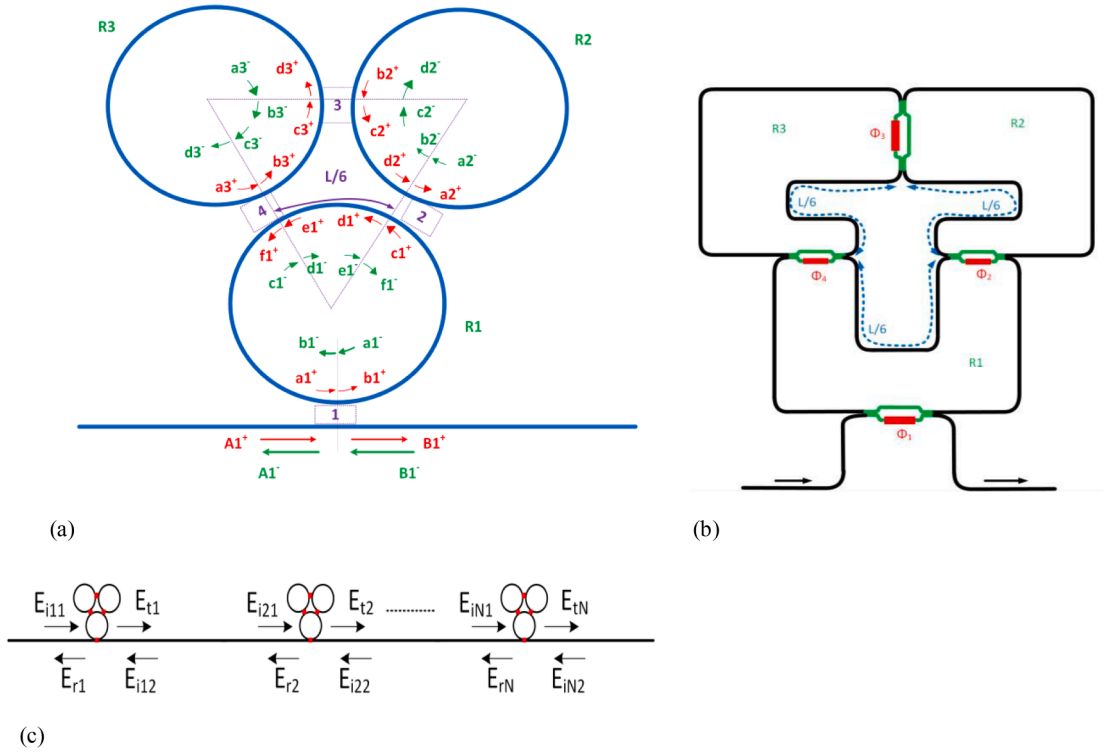

(a) (b) (c)

Fig. 1. Triple coupled MRRs; (a) detail field propagation with labelling. (b) suitable MRRs structure with MZI at coupling regions for tuning coupling coefficients. (c) cascaded triple MRRs with field propagations labelled (red colour indicates tunable elements). (For interpretation of the references to colour in this figure legend, the reader is referred to the web version of this article.)

$$\begin{pmatrix} f_1^+ \\ d_3^- \end{pmatrix} = \begin{pmatrix} t_4 & -jk_4 \\ -jk_4 & t_4 \end{pmatrix} \begin{pmatrix} e_1^+ \\ c_3^- \end{pmatrix}; \begin{pmatrix} d_1^- \\ b_3^+ \end{pmatrix} = \begin{pmatrix} t_4 & -jk_4 \\ -jk_4 & t_4 \end{pmatrix} \begin{pmatrix} c_1^- \\ a_3^+ \end{pmatrix} \quad (4)$$

Let γ_1 is the transmission factor of L/6-path and γ_2 is for 5/6*L path. Let θ_1 be the propagation phase for L/6 path and θ_2 be for 5/6*L path. The propagation phase relations are related as $\theta_1 = (\omega n_g L)/(6c_0)$; $\theta_2 = (5\omega n_g L)/(6c_0)$

Fields relations inside Ring 1:

$$\begin{aligned} &c_1^+ = \gamma_2^{1/2} e^{j\frac{\theta_2}{2}} b_1^+ \ , \ a_1^+ = \gamma_2^{1/2} e^{j\frac{\theta_2}{2}} f_1^+ \ , \ e_1^+ = \gamma_1 e^{j\theta_1} d_1^+ \\ &a_1^- = \gamma_2^{1/2} e^{j\frac{\theta_2}{2}} f_1^- \ , \ c_1^- = \gamma_2^{1/2} e^{j\frac{\theta_2}{2}} b_1^- \ , \ e_1^- = \gamma_1 e^{j\theta_1} d_1^- \end{aligned} \quad (5a)$$

Fields relations inside ring 2:

$$\begin{aligned} &b_2^+ = \gamma_2 e^{j\theta_2} a_2^+, \ d_2^+ = \gamma_1 e^{j\theta_1} c_2^+ \\ &a_2^- = \gamma_2 e^{j\theta_2} d_2^-, \ \ c_2^- = \gamma_1 e^{j\theta_1} b_2^- \end{aligned} \quad (5b)$$

Fields relations inside ring 3:

$$\begin{aligned} &a_3^+ = \gamma_2 e^{j\theta_2} d_3^+, \ \ c_3^+ = \gamma_1 e^{j\theta_1} b_3^+ \\ &a_3^- = \gamma_2 e^{j\theta_2} d_3^-, \ \ c_3^- = \gamma_1 e^{j\theta_1} b_3^- \end{aligned} \quad (5c)$$

The normalized transmitted electric field at port 2 is

$$\frac{B_1^+}{A_1^+} = \frac{m_{11}n_{22} - n_{12}m_{21}}{m_{22}n_{12} - m_{12}n_{22}} \quad (6a)$$

The reflected electric field at port 1 (input port) is

$$\frac{A_1^-}{A_1^+} = \frac{m_{11}m_{22} - m_{12}m_{21}}{m_{22}n_{12} - m_{12}n_{22}} \quad (6b)$$

Where the matrices related to the fields are given in (7) to (8) in the form of composite functions.

$$\begin{pmatrix} m_{11} & m_{12} \\ m_{21} & m_{22} \end{pmatrix} = \begin{pmatrix} \frac{x_{11}t_1 + x_{12}(t_1^2 + k_1^2)}{jk_1} & \frac{-x_{11} - x_{12}t_1}{jk_1} \\ \frac{x_{21}t_1 + x_{22}(t_1^2 + k_1^2)}{jk_1} & \frac{-x_{21} - x_{22}t_1}{jk_1} \end{pmatrix} \quad (7a)$$

$$\begin{pmatrix} n_{11} & n_{12} \\ n_{21} & n_{22} \end{pmatrix} = \begin{pmatrix} \frac{y_{11}t_1 + y_{12}(t_1^2 + k_1^2)}{jk_1} & \frac{-y_{11} - y_{12}t_1}{jk_1} \\ \frac{y_{21}t_1 + y_{22}(t_1^2 + k_1^2)}{jk_1} & \frac{-y_{21} - y_{22}t_1}{jk_1} \end{pmatrix} \quad (7b)$$

$$\begin{pmatrix} x_{11} & x_{12} \\ x_{21} & x_{22} \end{pmatrix} = \begin{pmatrix} \frac{-d_{12}d_{21} - d_{11}d_{22}}{c_{11}d_{21} - c_{21}d_{11}} & \frac{b_{11}b_{22} - b_{12}d_{21}}{a_{12}b_{22} - a_{22}b_{12}} \\ \frac{-d_{12}c_{21} - c_{11}d_{22}}{c_{11}d_{21} - c_{21}d_{11}} & \frac{b_{11}a_{22} - a_{12}b_{21}}{a_{12}b_{22} - a_{22}b_{12}} \end{pmatrix} \quad (7c)$$

$$\begin{pmatrix} y_{11} & y_{12} \\ y_{21} & y_{22} \end{pmatrix} = \begin{pmatrix} \frac{c_{22}d_{11} - c_{12}d_{21}}{c_{11}d_{21} - c_{21}d_{11}} & \frac{-a_{21}b_{12} - a_{11}b_{22}}{a_{12}b_{22} - a_{22}b_{12}} \\ \frac{c_{11}c_{22} - c_{12}c_{21}}{c_{11}d_{21} - c_{21}d_{11}} & \frac{-a_{12}a_{21} - a_{11}a_{22}}{a_{12}b_{22} - a_{22}b_{12}} \end{pmatrix} \quad (7d)$$

$$a_{11} = \frac{t_3 t_4 \gamma_2^{\frac{1}{2}} e^{j\frac{\theta_2}{2}}}{k_3 k_4} - \frac{(t_4^2 + k_4^2)\gamma_1 \gamma_2^{\frac{3}{2}} e^{j\left(\theta_1 + \frac{3}{2}\theta_2\right)}}{k_3 k_4}(t_3^2 + k_3^2) \quad (8a)$$

$$a_{12} = \frac{-t_3}{k_3 k_4} + \frac{t_4 \gamma_1 \gamma_2 e^{j(\theta_1 + \theta_2)}}{k_3 k_4}(k_3^2 + t_3^2) \quad (8b)$$

$$a_{21} = \frac{t_4 \gamma_1^{-1} \gamma_2^{-\frac{1}{2}} e^{-j(\theta_1 + \frac{1}{2}\theta_2)}}{k_3 k_4} - \frac{t_3(t_4^2 + k_4^2)\gamma_2^{\frac{1}{2}} e^{j\frac{1}{2}\theta_2}}{k_3 k_4} \quad (8c)$$

$$a_{22} = -\frac{\gamma_1^{-1}\gamma_2^{-\frac{1}{2}} e^{-j(\theta_1 + \frac{1}{2}\theta_2)}}{k_3 k_4} + \frac{t_3 t_4}{k_3 k_4} \quad (8d)$$

$$\begin{pmatrix} b_{11} & b_{12} \\ b_{21} & b_{22} \end{pmatrix} = \begin{pmatrix} \frac{t_2 \gamma_2^{1/2} e^{j\theta_2/2}}{jk_2} & -\frac{1}{jk_2} \\ \frac{(t_2^2 + k_2^2)\gamma_2^{1/2} e^{j\theta_2/2}}{jk_2} & -\frac{t_2}{jk_2} \end{pmatrix} \quad (8e)$$

$$c_{11} = \frac{t_2 t_3 \gamma_1 e^{j\theta_1}}{k_2 k_3} - \frac{(t_2^2 + k_2^2)\gamma_1^2 \gamma_2 e^{j(2\theta_1 + \theta_2)}(t_3^2 + k_3^2)}{k_2 k_3} \quad (8f)$$

$$c_{12} = \frac{-t_3 \gamma_2^{-\frac{1}{2}} e^{-j\frac{\theta_2}{2}}}{k_2 k_3} + \frac{t_2 \gamma_1 \gamma_2^{\frac{1}{2}} e^{j\left(\theta_1 + \frac{\theta_2}{2}\right)}(t_3^2 + k_3^2)}{k_2 k_3} \quad (8g)$$

$$c_{21} = \frac{t_2 \gamma_2^{-1} e^{-j\theta_2}}{k_2 k_3} - \frac{t_3(t_2^2 + k_2^2)\gamma_1 e^{j\theta_1}}{k_2 k_3} \quad (8h)$$

$$c_{22} = -\frac{\gamma_1^{-1}\gamma_2^{-3/2} e^{-j(\theta_1 + 3/2\theta_2)}}{k_2 k_3} + \frac{t_2 t_3 \gamma_2^{-1/2} e^{-j\theta_2/2}}{k_2 k_3} \quad (8i)$$

$$\begin{pmatrix} d_{11} & d_{12} \\ d_{21} & d_{22} \end{pmatrix} = \begin{pmatrix} \frac{t_4 \gamma_1 e^{j\theta_1}}{jk_4} & -\frac{\gamma_2^{-1/2} e^{-\theta_2/2}}{jk_4} \\ \frac{(t_4^2 + k_4^2)\gamma_1 e^{j\theta_1}}{jk_4} & -\frac{t_4 \gamma_2^{-1/2} e^{-\theta_2/2}}{jk_4} \end{pmatrix} \quad (8j)$$

$t_i^2 + k_i^2 \neq 1$ when the loss in the coupling region is considered, i = 1,2,3,4. And it is reduced by the loss factor α_i^2 as $t_i^2 + k_i^2 = 1 - \alpha_i^2$.

Cascading multiple N-number of coupled microring sets, as shown in Fig. 1(c), is useful in realizing bandpass filters with high extinction ratio, near to ideal shape factor, and flat-top filtering. We have to note the usage of the terms that the triple coupled microring resonators (TCMRR) are regarded as a single set, two cascaded TCMRRs are considered two sets and so on. The fields in the two-port TCMRR set designated by E_{in1} and E_{in2}, E_{tn}, and E_{rn} are incident, transmitted and reflected fields respectively, where n = 1, 2,.., N. Let T_N is the transmission from N^{th} coupled ring set, R_N is the reflection from the N^{th} TCMMR set, $T_{C(N)}$ is the total transmission from the N number of cascaded coupled TCMRR sets, $R_{C(N)}$ is the total reflection on the left side of the N^{th} set. For the n^{th} isolated (not cascaded) coupled set, the field relations are

$$E_{tn} = T_n E_{in1} + R_n E_{in2}; E_{rn} = T_n E_{in2} + R_n E_{in1} \quad (9a)$$

where R_n is the n^{th} amplitude reflection coefficient and T_n is the n^{th} amplitude transmission coefficient. Solving the above equation in terms of the input–output field relations, we have,

$$\begin{pmatrix} E_{in1} \\ E_{in2} \end{pmatrix} = \begin{pmatrix} -\frac{R_n}{T_n} & \frac{1}{T_n} \\ \frac{T_n^2 - R_n^2}{T_n} & \frac{R_n}{T_n} \end{pmatrix} \begin{pmatrix} E_{in2} \\ E_{tn} \end{pmatrix}, n = 1, 2, .., N \quad (9b)$$

For N number of cascaded systems,

$$\begin{pmatrix} E_{i11} \\ E_{r1} \end{pmatrix} = \begin{pmatrix} -\frac{R_1}{T_1} & \frac{1}{T_1} \\ \frac{T_1^2 - R_1^2}{T_1} & \frac{R_1}{T_1} \end{pmatrix} \begin{pmatrix} \frac{T_2^2 - R_2^2}{T_2} & \frac{R_2}{T_2} \\ -\frac{R_2}{T_2} & \frac{1}{T_2} \end{pmatrix} \cdots \begin{pmatrix} \frac{T_N^2 - R_N^2}{T_N} & \frac{R_N}{T_N} \\ -\frac{R_N}{T_N} & \frac{1}{T_N} \end{pmatrix} \begin{pmatrix} E_{iN2} \\ E_{tN} \end{pmatrix} \quad (9c)$$

When the input field is E_{i11}, the output at the N^{th} TCMMR set is obtained by setting $E_{iN2} = 0$ since there is no incident or input field at the output side. Therefore, the overall normalized transmission of the cascaded TCMMRs is $T_{cas(N)} = E_{tN}/E_{i11}$. It can be shown that the output transfer functions or normalized transmissions can be calculated

recursively, by considering the contributions from all reflected fields due to multiple reflections occurring among the TCMRR sets, as

$$T_{cas(N)} = \frac{T_{cas(N-1)}T_N}{1 - R_{cas(N-1)}R_N} \tag{9d}$$

Where $R_{cas(N)}$ is the reflected field contribution to the left of the N^{th} ring set:

$$R_{cas(N)} = \frac{R_N + \left(T_N^2 - R_N^2\right)R_{cas(N-1)}}{1 - R_{cas(N-1)}R_N} \tag{9e}$$

$R_{cas(N)}$is also computed recursively from previous cascaded TCMMR sets. For example, N = 3 (three TCMMR sets);$R_{cas(1)} = R_1, R_{cas(2)} = \frac{R_2+\left(T_2^2-R_2^2\right)R_{cas(1)}}{1-R_{cas(1)}R_2}, R_{cas(3)}\frac{R_3+\left(T_3^2-R_3^2\right)R_{cas(2)}}{1-R_{cas(2)}R_3}$

$$T_{cas(1)} = T_1, T_{cas(2)} = \frac{T_{cas(1)}T_2}{1 - R_{cas(1)}R_2}, T_{cas(3)} = \frac{T_{cas(2)}T_3}{1 - R_{cas(2)}R_3}$$

The transmitted T_n and reflected R_n of each TCMMR sets are computed from (6) to (8) when individual coupling coefficients t_1 to t_4 and k_1 to k_4 are tuned as required.

3. Numerical results and discussion

3.1. Methods

The device under consideration is designed on silicon-on-insulator (SOI) technology which is compatible with existing electronic foundries. The length of each microring is L = 300 μm which corresponds to a radius of R = 47.75 μm. The performance analysis of the device is carried out using MATLAB software. The effective and group refractive indices are calculated by using the multiphysics Lummerical MODE Solver software in SOI platform and the average group index is taken to be 4.2189 and the effective index is 2.4468. The standard silicon waveguide's maximum propagation loss is taken to be 3 dB/cm, and the bending and mode overlap losses are negligible when the radius of bend of silicon waveguide is greater than 10 μm (Chrostowski and Hochberg, 2015).

3.2. Performance analysis

3.2.1. Resonances of the device under different tuning conditions

The interaction between contra propagating modes has created various resonance patterns which are useful for realizing many functionalities. For clarification, We have started with forward propagating modes inside microrings and then allow small perturbation for backward modes to propagate in the microrings. Let us consider four cases. **Case-1:** only microring R1 is considered and the other two microrings R2 and R3 are decoupled (i.e., $t_2 = t_3 = t_4 = 1$) which means no coupling with R1 and hence no light can flow through R2 and R3. **Case-2:** two microrings are considered while the third microring is decoupled, i.e., not coupled. We can either decouple R2 or R3 but not R1. If we decouple R2, $t_2 = 1$, $t_3 = 1$ which means R1 and R3 are coupled in series. If we decouple R3, $t_3 = t_4 = 1$ which means R1 and R2 are coupled in series. **Case-3:** all of the three microrings are considered provided that the coupling in region three is not available, that is, $t_3 = 1$ so that no backward propagating modes are allowed inside the microrings. **Case-4:** all of the three microrings are mutually coupled by allowing t_3 different from one so that contra propagating modes are allowed to propagate inside the microrings. The transmission response in Fig. 2(a) depicts the forward propagating modes under case1, case 2 and case 3 conditions when we set t1 = 0.9, $t_2 = t_3 = 1$ or $t_3 = t_4 = 1$. The blue coloured response attributes to the single mciroring R1 coupled to a straight waveguide. The red coloured response is that of case-1 when R1 and R2 or R1 and R3 are considered. This response has two symmetrical resonances because of the presence of two coupled microrings. In the case of three coupled microrings, that is case-3 at $t_1 = 0.9$; $t_2 = t_4 = 0.5$; $t_3 = 1$, we see that the green coloured response exhibits three resonances. Resonances 2 and 3 are symmetrical with respect to resonance 1 which has the largest extinction ratio. Finally, when we perturb the system at coupling region 3, that is case-4 at $t_1 = 0.9$; $t_2 = t_4 = 0.5$; $t_3 = 0.98$, by small amount of $t_3 = 0.98$ which is very weak coupling, the splitting of resonances of case-3 occurs amounting to six resonances numbered as 1, 2, 3, 4, 5 and 6 as shown in Fig. 2(b). In other words, the splitting of the three resonances of case-3 is the result of the interaction between contra propagating modes due to coupling at region 3.

The responses for various tunable parameter configurations are depicted in Fig. 3. One can observe that the device exhibits diverse output optical power transmission spectra which are the result of multiple resonance interactions occurring due to the existence of two contra propagating optical modes inside the microring resonators. It is evident that we can control multiple resonance conditions by reconfiguring the coupling coefficients or applied voltages in the coupling regions. In Fig. 3(a) & (b), all three couped microrings have undergone resonance splitting which is tunable in bandwidth and extinction ratio. In Fig. 3(c) and (d), we can observe that the resonance splitting can be pushed to concentrate in a particular smaller frequency range and some resonances can be suppressed as well. Fig. 3(e) indicates that all three microrings are aligned to resonate in unison and Fig. 3(f) shows the split resonance of the unison resonance of Fig. 3(e). In Fig. 3(e) and (f), broader spectral ranges are caused by setting of identical coupling coefficients ($t_1 = t_2 = t_3 = t_4$). When we move from weak coupling to strong coupling, the number of resonance splitting modes reduce and completely destroyed when all coupling coefficients are less than or equal to 0.2 and the device behaves like conventional single microring with no resonance splitting modes. From Fig. 3(g), we can observe single

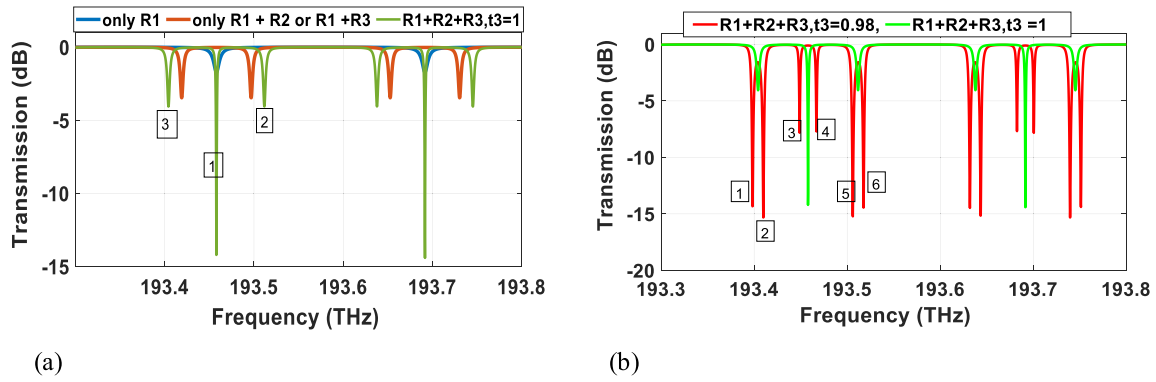

(a) (b)

Fig. 2. Transmission properties: (a) when only forward propagating mode is allowed to propagate (b) small perturbation is applied at coupling region 3 ($t_3 = 0.98$) for backward mode to propagate.

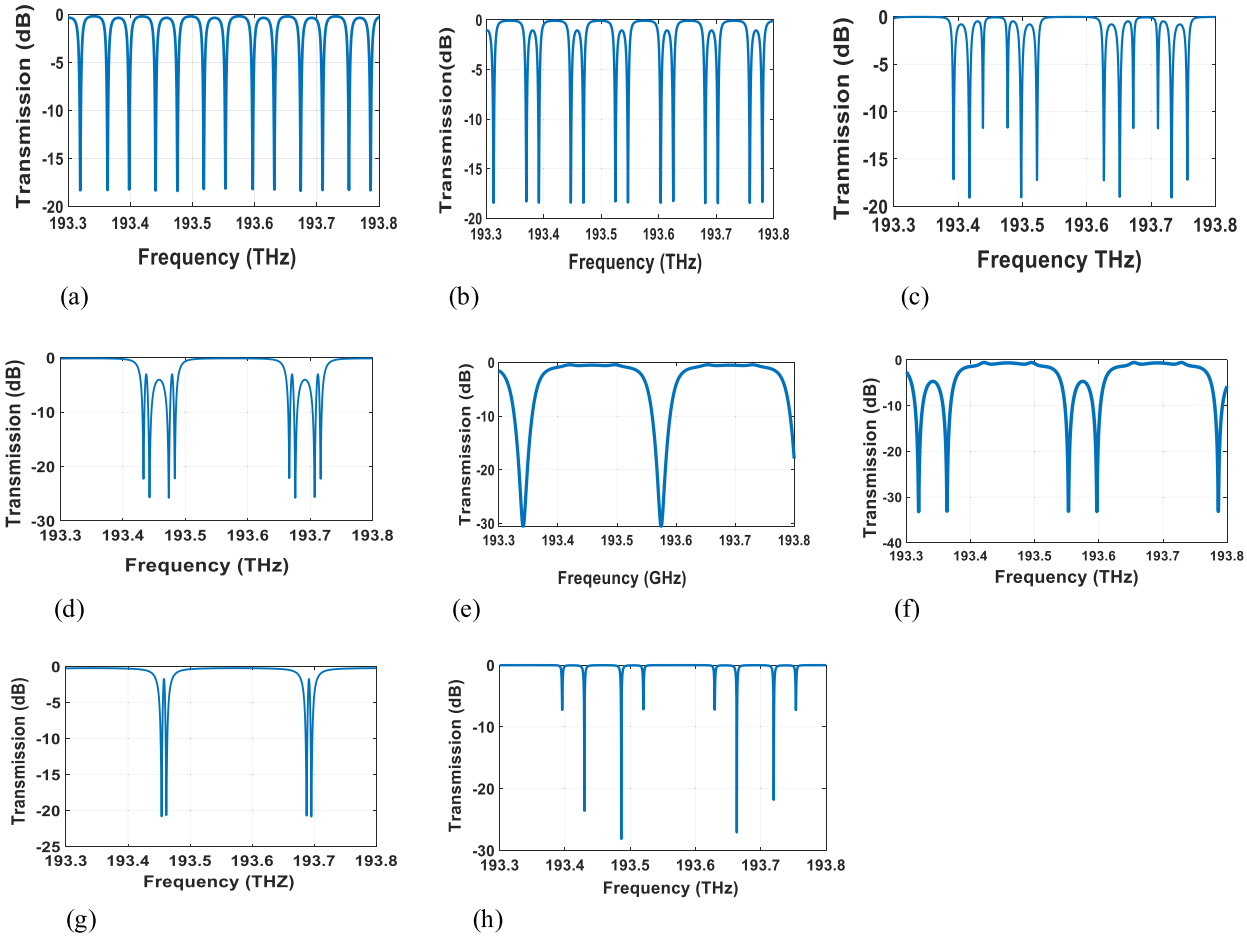

Fig. 3. Output transmission resonance patterns under different coupling coefficients. **(a)** $t_1 = 0.8$, $t_2 = 0.76$, $t_3 = 0.01$, $t_4 = 0.01$; **(b)** $t_1 = 0.8$, $t_2 = 0.9$, $t_3 = 0.01$, $t_4 = 0.01$; **(c)** $t_1 = 0.84$, $t_2 = 0.75$, $t_3 = 0.75$; $t_4 = 0.4$; **(d)** $t_1 = 0.01$, $t_2 = 0.8$, $t_3 = 0.84$, $t_4 = 0.91$; **(e)** $t_1 = t_2 = t_3 = t_4 = 0.2$ **(f)** $t_1 = t_2 = t_3 = t_4 = 0.3$ **(g)** $t_1 = 0.01$, $t_2 = 0.95$, $t_3 = 0.95$, $t_4 = 0.01$; **(h)** $t_1 = 0.96$, $t_2 = 0.67$, $t_3 = 0.67$, $t_4 = 0.67$.

microring split resonance is achieved by controlling tunable parameters. In Fig. 2(h), we can observe deep resonance frequency notches which are helpful properties to design notch filters.

3.2.2. *Utilization of various resonance features for different applications*

3.2.2.1. Filtering. Filtering functionality is an integral part of modern-day communication networks such as multiplexing/demultiplexing of multiple channels (Uetsuka, 2004; Manganelli et al., 2017), in equalizing and compensating harmful dispersion effects (Inoue et al., 1991; Chryssou, 2000), in microwave signal processing (Lenz and Madsen, July 1999) because of excellent performance such as low loss, light weight, wideband frequency tunability, immunity to electromagnetic interference.

Microring resonator-based filters play a crucial role in designing reconfigurable high pass, bandpass and notch type of filtering functions. For example, a 25 GHz center frequency tunable microwave photonic notch filter and high RF rejection ratio is achieved by using a dual-drive Mach Zender modulator and a microring resonator (Zheng et al., 2019). But, the use of quadrature bias and phase modulator complicate the design and control. Integrated RF photonic notch filter on a Si3N4 chip, with high rejection (>50 dB), center frequency tuning range of 1–12 GHz is proposed using two under coupled and over coupled microring resonators (Liu et al., 2017). But maintain two microring resonators in under couped and over coupled states may be difficult. A silicon nitride-based microwave photonic notch filter with four microrings cascaded (two in over coupled state and two under coupled state), with 8 dB RF gain, with 50 dB rejection ratio, up to 50 GHz center frequency tunability range has been proposed (Liu et al., 2017). The authors reported high performing notch filter except the number of microring counts, that is, four microrings should be tuned and controlled in over coupled and under coupled states. Our proposed device has comparable performance with those reported on literature with 50 dB rejection ratio and 22.5 GHz center frequency tunability. Besides, the advantage of our proposed system, as compared to others in the literature with single frequency band (Little, Oct., 2004; Hu et al., 2012; Geremew and Talabattula, 2021), is that by cascading higher orders bandpass filtering with two frequency bands, with 3 dB bandwidths of 37.7 GHz and 95.2 GHz for individual microring resonator length of 300um, have been achieved. When the length changes the bandwidths changes. But, in the literature only single bandwidth bandpass filters are realized by cascading higher orders of microrings. Finally, our device can be programmed as bandpass and bandstop functionalities without transmission port change, that is, the outport can act as a switch.

Reconfigurable multiple resonances and their splitting features associated with the device provide useful filtering performance characteristics such as high out of band rejection, flat-top bandwidth, and near to ideal shape factor. The device can perform as bandpass, bandstop filter and notch filter. This means the signal with the same frequency range can be allowed to pass and can be blocked just by programming the coupling coefficients. The applications of the diverse resonance features are demonstrated in Fig. 4(a) and Fig. 4(b). In Fig. 4(a), one can observe reconfigurable dual band frequency bandpass and bandstop filters. Besides, the same port can be reused as a reconfigurable switch.

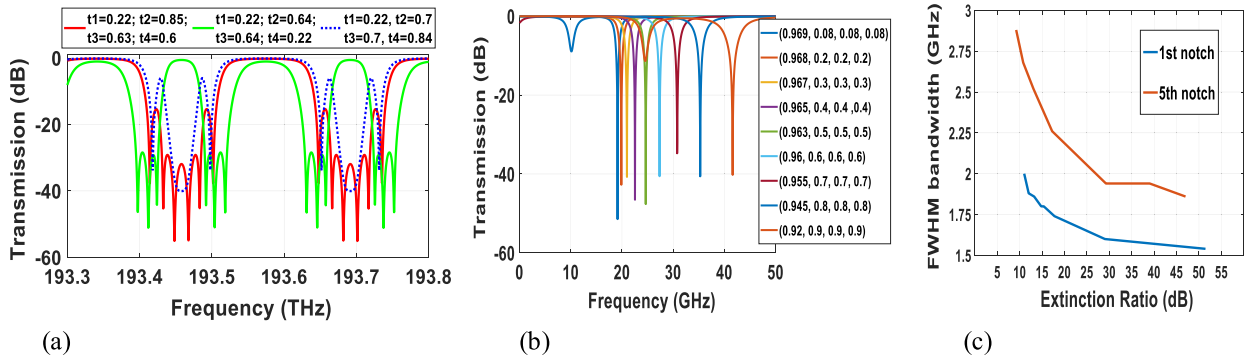

Fig. 4. Filtering applications: (a) as bandpass and bandstop filters with dual frequency bands. (b) as tunable notch filter with reconfigurability. (c) full width half maximum bandwidth vs extinction ratio (FWHM).

In Fig. 4(b), the device is reconfigurable for multiple frequency notches. As we can observe, the notch center frequency is tunable over 22.5 GHz band. The tunability of the extinction ratio and 3 dB bandwidth is indicated for the first and fifth notches as depicted in Fig. 4(c). For 1st notch, the bandwidth ranges from 2 to 1.54 GHz, and for that of 5th notch varies from 2.88 to 1.86 GHz. The bandwidth is measured over a minimum extinction (ER) ratio of 10 dB for both cases; the maximum ER extends to 50 dB. Therefore, the device can be used as a tunable microwave photonic notch filter by connecting photodetector to the output of the device.

Using (6)–(9), the bandpass optical transmission spectra responses of cascaded 2nd, 3rd and 4th orders are computed and depicted in Fig. 5 (d) for frequency band one centered at 193.455 THz when the coupling coefficient sets of $\{t_1, t_2, t_3, t_4\}$: {[0.37, 0.52, 0.73, 0.4], [0.37, 0.5, 0.78, 0.4], [0.37, 0.5, 0.73, 0.4], [0.4, 0.52, 0.73, 0.4]} respectively are optimized for TCMRR sets 1,2, 3 and 4 (or 1st , 2nd ,3rd ,4th orders) , and in Fig. 5(f) for frequency band two centered at 193.557 THz when the coupling coefficient sets of $\{t_1, t_2, t_3, t_4\}$: {[0.25, 0.67, 0.67, 0.85], [0.32, 0.7, 0.7, 0.4], [0.34, 0.67, 0.67, 0.86], [0.2, 0.64, 0.64, 0.88]} respectively are optimized for coupled ring sets 1,2, 3 and 4. In Fig. 5(b) and (d), the 4th order responses with extinction ratio greater than 60 dB are shown for the two frequency bands. For the frequency band one, the performances of the three orders in terms of out-of-band rejection ratio, 3 dB flat-top bandwidth, shape factor and flat-top loss are (30 dB, 37.3 GHz, 0.89, 0.34 dB), (43 dB, 35.73 GHz, 0.86, 0.53 dB), and (62.54 dB, 35.7 GHz, 0.88, 0.75 dB) respectively for 2nd , 3rd and 4th orders. For frequency band two, the performances of the three orders in terms of out-of-band rejection ratio, 3 dB flat-top bandwidth, shape factor and flat-top loss are (24 dB, 95.7 GHz, 0.91, 0.76 dB), (41.7 dB, 94.2 GHz, 0.91, 1.25 dB), and (64.3 dB, 95.2 GHz, 0.92, 1.35 dB) respectively for 2nd , 3rd and 4th orders .Here, shape factor is defined as the bandwidth ratio of -3 dB to -10 dB transmissions, and it is a measure of how close the bandpass response is to the ideal shape factor of unity (rectangular response).

Cascading reflective type filters has the tendency of reducing bandwidth when we move from second order to third order, but negligible from third order to fourth order transition. The main advantage of cascading multiple orders is to get high out-of-band rejection ratio (RR),

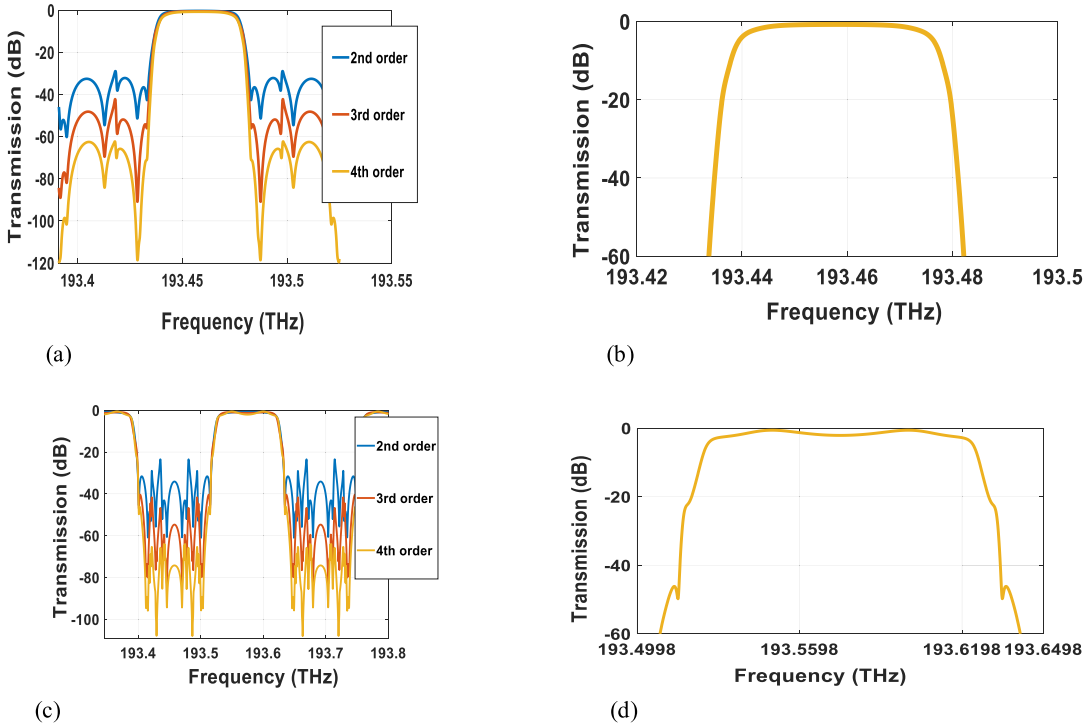

Fig. 5. Filtering applications: (a) bandpass response of cascaded system at frequency band one. (b) 4th order bandpass filter response for frequency band one. (c) bandpass response of cascaded system at frequency band two for various cascade order. (d) 4th order bandpass filter response of frequency band two.

and improved shape factor. However, the effect in bandwidth changes and loss is negligible for orders higher than two. If we consider fourth order filter, for example, the most important observations are 3 dB bandwidth of 37.7 GHz for frequency band one as shown in Fig. 5(b) and 95.2 GHz for frequency band two, shape factor of 0.9 for the first band and 0.88 for the second band as shown in Fig. 5(d). Besides, an FSR of 234 GHz is achieved for both bands and Q-factor is defined as the ratio of operation frequency to FWHM bandwidth. If we select operation frequency of 193.46 THz for band one and 193.567 THz for band two, we have Q-factors of 5,131 and 2033 respectively for band one and two. We can note that the ripple less than 1 dB is observed in frequency band two. The out-of-band rejection ratio is more than 60 dB for both bands. The shape factors are near to ideal shape factor of unity. We have to note that the flat-top bandwidth is not tunable in this type of reflective filter types; we can design only for fixed two band frequencies. But the bandwidth is inversely proportional to the length/radius of the microrings, that is, by increasing the length of the coupled ring sets we can reduce the bandwidth and vice versa. The main advantage of our proposed system as compared to others in the literature is that by cascading higher orders bandpass filtering with two frequency bands can be performed. But, in the literature (Little, Oct., 2004; Hu et al., 2012; Geremew and Talabattula, 2021), only single bandwidth bandpass filters are realized by cascading higher orders of rings.

3.2.2.2. Optical logical operation. Logical operation is carried out in optical domain through applied control voltages. The device can be programmed to operate as an optical switch by probing control electrical voltage signals which in turn alter the coupling coefficients of the device. The different combination of control signals represents the classical logical gates such AND, OR, XOR and XNOR. For certain combination of control voltages, the device can operate as bandpass (logic high) and for other combinations it can operate as bandstop (logic low). Classical electronic circuits have speed limitations in handling logical operation of high frequency and wideband microwave signals. Therefore, logical operation can be implemented through modulation of wideband microwave signals by optical carrier. Logical switching of microwave signals using optical circuits is useful for the future of high-speed radio-over-fiber communications such as 5G and 6G networks.

Commonly used electronic logic gates are demonstrated using optical switching. In (Godbole et al., 2016), five cascaded MMRs employed to design all optical scalable logic gates using optical kerr effect. Electrically controlled optical logic directed decoder was implemented using two MRRs (Chen et al., 2014). A single four port reflective type MRR (Pan et al., 2020) was demonstrated for XNOR gate operation by electrical pulse control, but the switching is narrowband notch response for bandstop and the power is lost in the three ports: loss in loop reflector used in port 3, reflected back to the source at port 1 and wasted at port 2 (through port). Unlike two input narrowband logical operations demonstrated in the literature, our proposed device can perform as three input logical operator and it can switch wideband microwave frequency signals optically.

The diagram depicted in Fig. 6 is adapted for operation as optical logic gate for microwave signal switching. The control voltages are applied on tuners or heaters above one of the arms of MZIs. A laser diode (LD) modulates an RF frequency of f_{RF} and the modulated optical signal is fed to the triple coupled microring resonators. Finally, RF signal is detected after optical logical operation. The control voltages V_1, V_2, V_3 and V_4 are applied on one of the arms of MZIs to tune the corresponding coupling coefficients t_1, t_2, t_3 and t_4.

The most important logical operations, XOR and XNOR, will be illustrated in our proposed system. The tables A, B, and C show the logic truth table for three input XOR, two input XOR and two input XNOR with the corresponding coupling coefficient settings which are equivalent to applied control voltages. For the three input XNOR logical operation, the coupling coefficient t_1 is set at a fixed value of 0.22, and

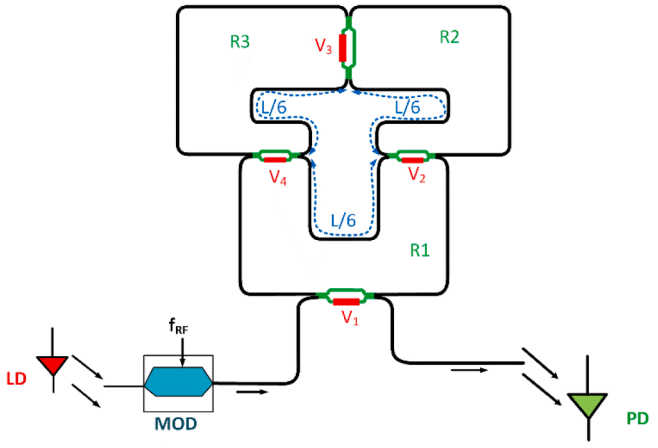

Fig. 6. Typical architecture for optical logical gate to control RF/microwave signals: LD (laser diode), MOD: modulator, PD: photodetector.

(t_2, t_3, t_4) are used to implement logic operations. All self-coupling coefficients with $t < 0.5$ are set to be tuned at high voltages: logic high, and all self-coupling coefficients with $t > 0.5$ are set to be tuned at low voltages: logic low. As We can observe in Table 1, for three input XOR, t_1 is set fixed at 0.22, t_2, t_3 and t_4 control logical operation. For example, when (t_2, t_3, t_4) = (0.85,0.7,0.7) the device acts as a bandstop which similar to electrical logic input of (0,0,0) for output logic low or 0 and when (t_2, t_3, t_4) = (0.7, 0.7, 0.3) the device acts as a bandpass which similar to electrical logic input of (0,0,1) for output logic high or 1. For the two-input XOR, in Table 2, t1 and t4 are fixed at 0.22 except when all inputs are high t_4 is set at 0.83, and t_2 and t_3 are used to implement logical operation. Similarly, for the two input XNOR operation, Table 3, t1 and t4 are fixed at 0.22 and t_2 and t_3 are used to implement the logical operations.

- All self-coupling coefficients with $t < 0.5$ are set to be tuned at high voltages [logic high] and all self-coupling coefficients with $t > 0.5$ are set to be tuned at low voltages [logic low].

The optical switching outputs which represent logical operations are shown in Fig. 7, with outputs values with loss greater than 10 dB are regarded as logical low (zero) and all outputs less than 10 dB are regarded as logical high. As we see from the figures, the outputs for logic low have a loss greater than 20 dB and outputs with logic high have loss less than 1 dB. RF signals with a span of 12 GHz bandwidth (from optical frequency of 193.452 THz to 193.464 THz in Fig. 7) can be modulated. The absolute RF frequency can be any value but the bandwidth should not exceed 12 GHz; that is why we claim that our proposed structure can operate at wideband RF frequency band.

3.2.2.3. Optical true time delay lines. Microring resonators are well researched for optical true time delay in microwave optical phased array antenna beamforming because of continuous tunability of beam steering

Table 1
Truth table three input-XOR gates (t_1 = 0.22 fixed).

t2	t3	t4	Analog output	input-1	Input-2	Input-3	Logical output
0.85	0.7	0.7	Bandstop	0	0	0	0
0.7	0.7	0.3	Bandpass	0	0	1	1
0.85	0.2	0.95	Bandpass	0	1	0	1
0.8	0.3	0.4	Bandstop	0	1	1	0
0.3	0.7	0.7	Bandpass	1	0	0	1
0.1	0.88	0.1	Bandstop	1	0	1	0
0.22	0.4	0.88	Bandstop	1	1	0	0
0.22	0.22	0.22	Bandpass	1	1	1	1

Table 2
Truth table two input-XOR gate ($t_1 = 0.22 = t_4$, fixed).

t2	t3	t4	Analog-output	Input-1	Input-2	Logical output
0.9	0.4	0.22	bandstop	0	0	0
0.6	0.4	0.22	bandpass	0	1	1
0.3	0.7	0.22	bandpass	1	0	1
0.4	0.4	0.83	bandstop	1	1	0

Table 3
Truth table two-input xnor gate ($t_1 = t_4 = 0.22$ fixed).

t2	t3	Analog-output	Input-1	Input-2	Logical output
0.7	0.7	Bandpass	0	0	1
0.9	0.45	Bandstop	0	1	0
0.15	0.92	Bandstop	1	0	0
0.22	0.22	Bandpass	1	1	1

angle coverage, small footprint for large array beamforming, and low loss (Meijerink et al., 2010; Choo et al., 2018; Leimeng Zhuang et al., 2010; Burla, et al., 2014; Ortega and Mora, 2016). However, conventional MMRs have very narrow bandwidth and constant delay and bandwidth product constant. This means if the time delay is increased by tuning coupling coefficient, the bandwidth reduces dramatically and vice versa. This phenomenon causes group delay dispersion and results in harmful distortion of the wideband microwave signals, resulting loss of the signal information during decoding process. Therefore, it is important to break the bandwidth bottleneck and dispersive nature of conventional ring resonators by using reflective type coupled microring resonators.

In this section, we demonstrate theoretically the group delay and transmission performance characteristics of three mutually coupled MRRs for microwave optical beamforming. The proposed device exhibits flat top large bandwidth which is useful property in realizing optical beamforming of RF/microwave signals. The transmission phase information is extracted from (6a) and its response is depicted in Fig. 8 (a) for various coupling coefficient settings. The coefficients, $t_1 = t4$ and $t_2 = t_3$, are optimized in order to get linear phase variation and simplify tuning complexity. Besides, t_1 and t_4 are limited between 0 and 0.12, and t_2 and t_3 varies between 0 and 1. We can observe two types of phase responses: one with positive slope (negative group delay) and another with negative slope (positive group delay). Here, slope refers to the first derivative of phase information with respect to frequency. Moreover, one can observe from Fig. 8(a) that the positive slope phase variation occurs over wide frequency range while negative slope occurs within small frequency range. Besides, positive slope frequency range reduces with increasing identical coupling coefficients t_2 and t_3.

The group delay response for reflective type triple coupled microring resonators is computed numerically, using finite difference approximation algorithms, by differentiating the phase information extracted from transmission equation given in (6a); deriving analytical solution for group delay is cumbersome because of the transmission equation complexity. We have to note that, by definition, the group delay is the negative of the slope of phase variation with frequency. In RF and microwave applications of phased array beamforming, the successive differential phase variation and group delay variation between successive antenna elements play an important role in scanning diverse steering angles, and the photodetector doesn't care about the sign of group delay. Therefore, we consider the positive slope phase variation for group delay performance analysis since our goal is wideband frequency coverage and wideband flat top delay response achievement.

As we can observe from Fig. 8(a), the phase of the optical signal varies linearly over wide range of optical frequency which results in constant time group delay response, Fig. 8(b), since group delay is the first derivative of phase information. The wideband flat-top delay response is due to the presence of contra propagating optical signals or electric field modes inside the MRRs. The slow and fast light interaction occurring during tuning of coupling coefficients is the cause of the wideband group delay response. Fig. 8(c) indicates that the transmission is peak at center frequency where the peak delay occurs for the same reconfigurable parameters as of Fig. 8(a). Fig. 8(d) and (e) show the three-dimensional (3D) phase and group delay responses with respect to detuned RF frequency and coupling coefficient $t = t_2 = t_3$. When coupling coefficient is increased, group delay increases but its bandwidth decreases. We have to note that the tuning parameters t_4 is necessarily fixed to be less than or equal to 0.12 since the insertion loss is small for those range of values. The parameter t_1 controls the ripple and hence it is required to set it small value to reduce delay ripple over flat-top region. Setting t_1 less than 0.12 gives small ripple. The remaining parameters $t_2 = t_3 = t$ is same for all delay and hence we need to tune only one variable t to get the desired time delay. The delay and bandwidth versus coupling coefficient $t = t_2 = t_3$, when t_1 and t_4 are fixed at 0.12, is depicted in Fig. 8(f).

For small value of t, we have large delay bandwidth calculated within 1 ps difference of peak delay), but small-time delay and vice versa. For example, when t = 0.12, the delay is 10 ps and bandwidth is 78 GHz, when t = 0.8, we have delay of 26 ps with 15 GHz bandwidth and even for large time delay near to 58 ps at t = 0.95, we obtain 3 GHz bandwidth. In conventional microring resonators, We cannot achieve such large bandwidth by cascading the same number of three microrings. Finally, We have to note that to get tunable time delay with minimum ripple we set t_1 less than 0.12. However, for t_1 less than 0.12 we cannot get a delay less than 10 ps, and hence it is also required to tune t_1 from 0.2 to 0.98 to get a small-time delay less than 10 ps by setting $t_2 = t_3 = t_4 = 0.1$. The three microrings system gives a delay of 0.006 ps when $t_1 = 0.999$, $t_2 = t_3 = t_4 = 0.1$ and 0.043 ps when $t_1 = 0.98$, $t_2 = t_3 = t_4 = 0.1$. But the single microring gives a minimum of 4.26 ps when $t_1 = 0.001$, $t_2 = t_3 = t_4 = 1$(only single ring-R1) and 4.3 ps when $t_1 = 0.01$, $t_2 = t_3 = t_4 = 1$. Thus, the three microrings system can be tunable starting from near 0 ps and the single microring is tunable starting from a minimum of 4.26 ps.

Binary-tree structured and continuously tunable OBFNs have been implemented using cascading large MRRs (Meijerink et al., 2010; Choo et al., 2018; Leimeng Zhuang et al., 2010; Burla, et al., 2014; Ortega and

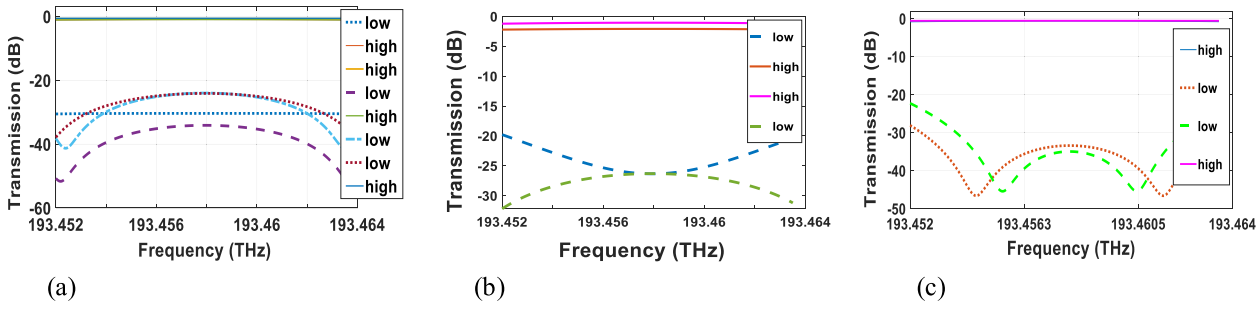

Fig. 7. Logical operations output: (a) Three input XOR logic gate output. (b) two -input XOR logic gate output. (c) two input XNOR logic gate output.

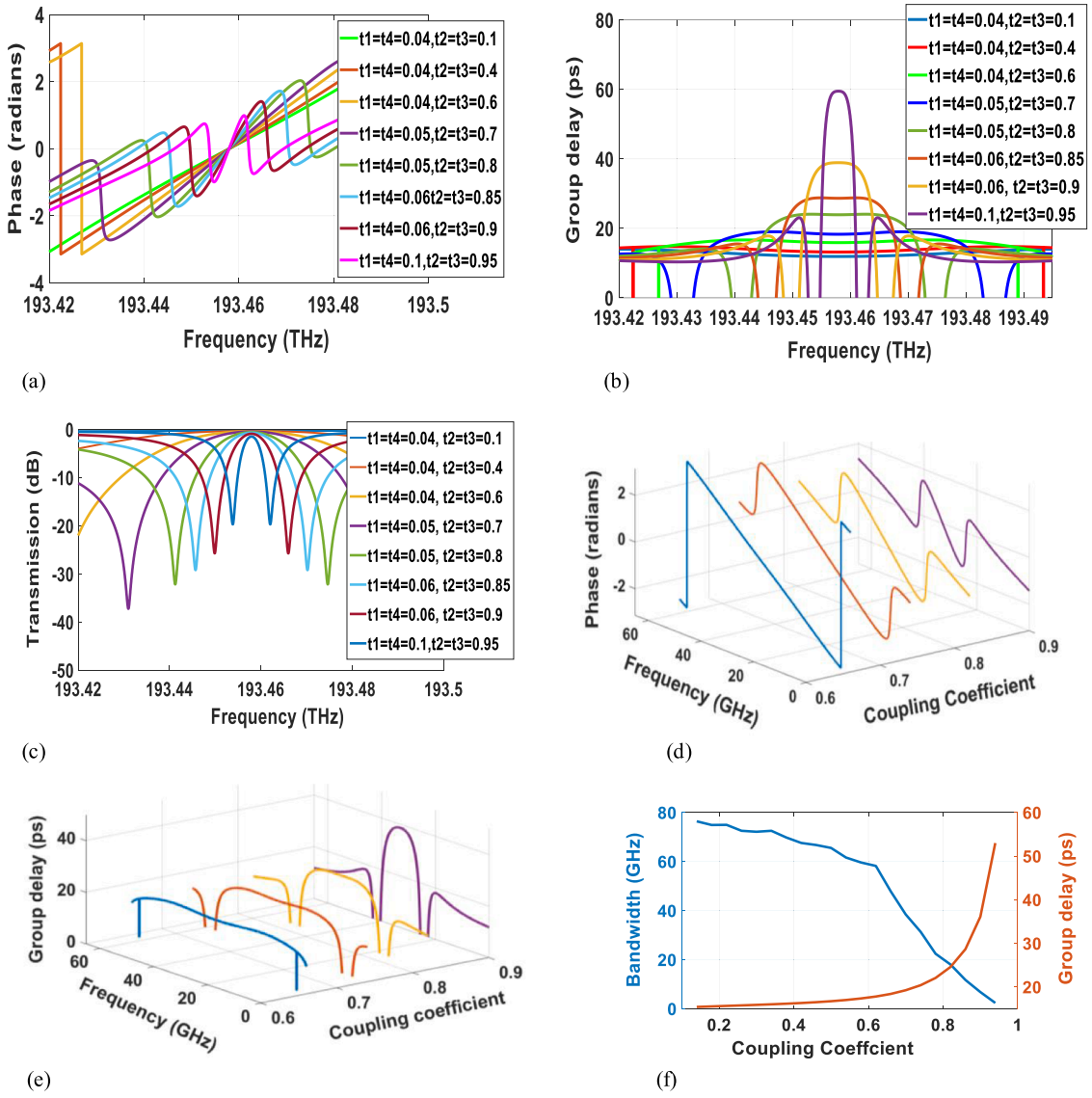

Fig. 8. Demonstration of device performance as optical true time delay line. **(a)** Phase variation with frequency for various coupling coefficient settings. b) group delay for the same coupling coefficient settings as (a). (c) transmission for the same coupling coefficient settings as (a). (d) 3D visualization of phase with detuned RF frequency and coupling coefficient ($t_2 = t_3 = t$ varies). (e) 3D visualization of group delay with detuned RF frequency and coupling coefficient response (($t_2 = t_3 = t$ varies). (f) 1-ps time delay bandwidth and time delay vs coupling coefficient ($t_1 = t_4 = 0.12$ fixed, $t_2 = t_3 = t$ varies).

Mora, 2016). Cascading of MRRs has twofold advantages: the first is to reduce dispersion and enhance bandwidth, and the second is to increase group delay. Each MRR requires two tuners: one for coupling coefficient to control time delay and the second for resonance position to control the bandwidth. If we have, for example, 20 cascaded MRRs, we have to optimize 40 variables to obtain the desired time delay and operational bandwidth. This high-level multi-objective optimization highly complicates the tuning. However, in our design we have only one variable for tuning. Since sufficient bandwidth is already achieved by the single set reflective type TCMRRs, cascading is required only for increasing the time delay. Progressive linear addition of time delays for all antenna elements is easily achieved by cascading many TCMMRs once a tuning parameter t is determined from the desired differential time delay between successive antenna elements.

To illustrate the how TCMMRs are applied in optical beamforming of RF/microwave signals, let us consider a 4-element linear antenna array with its beamforming architecture as shown in Fig. 9(a). Each time delay generation unit (one TCMMRs) is coupled to a common waveguide to which the RF/microwave signal modulated optical signal is applied.

The waveguides feeding antenna elements are coupled with the common waveguide so that signals with the corresponding delays can be fed to each antenna. The power coupling ratio can be controlled to feed all antennas with the same power. The red colour indicates the tunable coupler and MZI. Let τ be the time delay generated by one TCMRR set. Then the signal, fed to each antenna elements $\{AE_1, AE_2, AE_3, AE_4\}$, see progressive time delays $\{0, \tau, 2\tau, 3\tau\}$ respectively, where antenna element AE_1 is used as a reference element with zero delay.

We illustrate design example for linear antenna array. In cascaded TCMMR sets, the time delay is computed using (6) and (9) considering the effect of reflection from each set. We assume half wavelength antenna spacing at microwave frequency of $f_0 = 28$ GHz. The differential delay between antenna elements is $\Delta\tau = d^{*}sin(\theta_{max})/c_0 = \sin(\theta_{max})/2f_0$. Maximum beam steering occurs at $\theta_{max} = 90^{\circ}$. Then $\Delta\tau_{max} = 1/2f_0 = 18ps$; the delays on antenna elements are 0, 18 ps, 36 ps, and 54 ps taking the first element as a reference with zero delay. The delay generated by the device for all antenna elements is depicted in Fig. 9(b) with a flat response of 18 GHz bandwidth. For the fixed values of $t_1 = t_4 = 0.12$, the tunning parameters ($t = t_2 = t_3$) to get 18 ps delays are

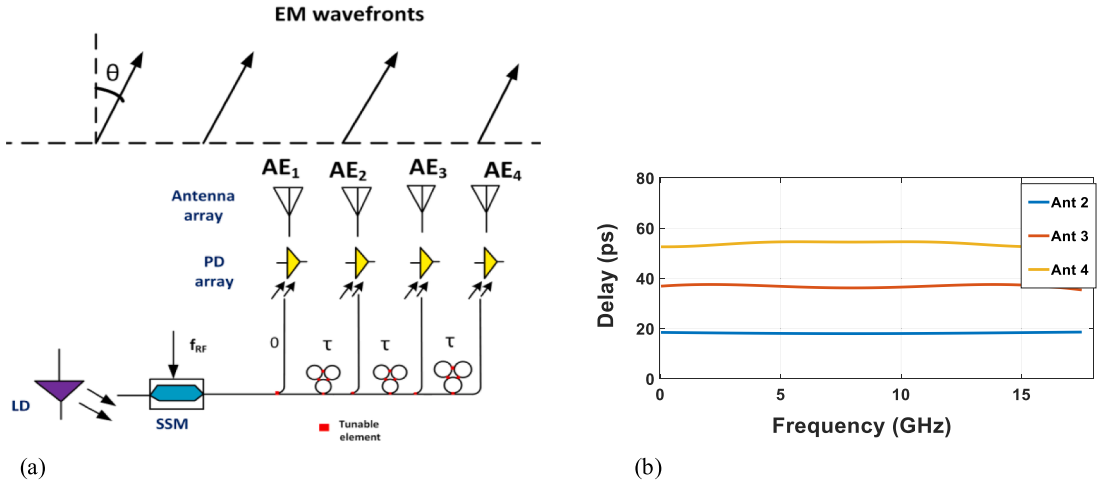

Fig. 9. Typical architecture for optical true time delay line. (a) linear antenna array (b) delay responses generated for 4-element array at maximum scanning angle 90 degrees. SSM: single sideband modulator, LD: laser diode, PD: photodetector, AE: antenna element, EM: electromagnetic, Ant: antenna.

optimized to be $t_2 = t_3 = 0.7$. The same tuning parameters are applied for the 36 ps and 54 ps since the time delays are linearly spaced. The parameters t_1 and t_4 can be fixed at 0.12 as evidenced from Fig. 8 and only $t_2 = t_3 = t$ should be optimized. This means that a single tuning voltage $V = V_2 = V_3$ and another fixed voltage $V_f = V_1 = V_4$ is applied to all delay generation units. In this scheme, tuning complexity is significantly reduced since only single variable tuning is required to change time delay continuously. The first antenna uses one set of TCMMRs, the second antenna uses two sets of TCMRRs and the third antenna uses three set TCMMRs. As we see that the delay units are shared among antenna elements. For example, antenna 3 shares TCMMRs that are used by antenna 2 and antenna 4 shares TCMRRs that are used by antenna 3. This sharing of delay generation units reduces hardware complexity. Individual delay units can generate a delay near to 0 ps which means that the minimum scanning angle is near 0 degree. Therefore, any angular range can be scanned continuously with reconfiguration of coupling coefficients.

4. Conclusions

In this paper, we have theoretically demonstrated the performances of reflective type triple coupled microring resonators (TCMMRs) for reconfigurable photonic based systems such as optical filtering, optical logical operations, and optical true time delay lines. TCMRRs can function as dual band bandpass filters with wide bandwidths of 37.5 GHz and 95.2 GHz, with shape factors of 0.9 which is near to ideal value of unity and with extinction ratio exceeding 60 dB. The bandwidths change when we change the length of individual micro rings. The device can function as the notch filter with 22.5 GHz wideband center frequency tunability, with extinction ratio of 50 dB, and with 3 dB bandwidth between 1.5 GHz and 3 GHz. Moreover, the device can be reconfigured to operate as two or three input optical local gate by probing control electrical voltage signals which in turn alter the coupling coefficients of the device. Finally, the proposed device can be a good candidate to function as optical true time delay line for optical beamforming of phased array antenna in RF/microwave applications. This because the device exhibits flat top delay response with wideband bandwidth range of 3 GHz to 78 GHz which varies depending on the setting of tunable coupling coefficient. The group delay of a single TCMMR can be tuned from near to zero ps to 60 ps, and cascading multiple TCMRRs increases the group delays.

Declaration of Competing Interest

The authors declare that they have no known competing financial interests or personal relationships that could have appeared to influence the work reported in this paper.

Acknowledgements

This work is supported by Indian Institute of Science, Department of Electrical Communication Engineering, Applied Photonics Lab.

References

Zhang, L., Yang, J., Li, Y., Song, M., Beausoleil, R., Willner, A., 2008. Monolithic modulator and demodulator of differential quadrature phase-shift keying signals based on silicon microrings. Opt. Lett. 33, 1428–1430.

P. Toumasis G. Giannoulis G. Poulopoulos K. Kanta D. Apostolopoulos H. Avramopoulos 39 6 2021 1662 1671.

L. Zhang et al., "Generating spectral-efficient duobinary data format from silicon ring resonator modulators," 2008 34th European Conference on Optical Communication, Brussels, Belgium, 2008, pp. 1-2, doi: 10.1109/ECOC.2008.4729212.

Z. Yao et al., "Integrated Silicon Photonic Microresonators: Emerging Technologies," in IEEE Journal of Selected Topics in Quantum Electronics, vol. 24, no. 6, pp. 1-24, Nov.-Dec. 2018, Art no. 5900324, doi: 10.1109/JSTQE.2018.2846047.

Zhu, H.H., Yue, Y.H., Wang, Y.J., Zhang, M., Shao, L.Y., He, J.J., Li, M.Y., 2017. High-sensitivity optical sensors based on cascaded reflective MZIs and microring resonators. Opt. Express 25 (23), 28612. https://doi.org/10.1364/OE.25.028612.

Sun, R. Kumar, M. Sakib, J. B. Driscoll, H. Jayatilleka and H. Rong, "A 128 Gb/s PAM4 Silicon Microring Modulator With Integrated Thermo-Optic Resonance Tuning," in Journal of Lightwave Technology, vol. 37, no. 1, pp. 110-115, 1 Jan.1, 2019, doi: 10.1109/JLT.2018.2878327.

F. Mohammadi, V. Ahmadi and M. Gandomkar, "Dynamics and Frequency Response of Microring-Based Optical Modulator Considering Nonlinear Effects," in Journal of Lightwave Technology, vol. 30, no. 23, pp. 3720-3726, Dec.1, 2012.

Wu, J., Peng, J., Liu, B., Pan, T., Zhou, H., Mao, J., Yang, Y., Qiu, C., Su, Y., 2016. "Passive silicon photonic devices for microwave photonic signal processing. Opt. Commun. 373, 44–52.

Capmany, J., Novak, D., 2007. Microwave photonics combines two worlds. Nature Photon 1 (6), 319–330.

Little, B.E., et al., 2004. Very high-order microring resonator filters for WDM applications. IEEE Photon. Technol. Lett. 16 (10), 2263–2265.

T. Hu et al., "Thermally Tunable Filters Based on Third-Order Microring Resonators for WDM Applications," in IEEE Photonics Technology Letters, vol. 24, no. 6, pp. 524-526, March15, 2012.

G. Fekadu Mihret, T.Srinivas ,"Performance analysis of reconfigurable multifunctional photonic filters using triple coupled microring resonators,"Optics Communications, Vol.486, 2021.

Cardenas, J., Foster, M.A., Sherwood-Droz, N., Poitras, C.B., Lira, H.L.R., Zhang, B., Gaeta, A.L., Khurgin, J.B., Morton, P., Lipson, M., 2010. Wide-bandwidth continuously tunable optical delay line using silicon microring resonators. Opt. Express 18 (25), 26525. https://doi.org/10.1364/OE.18.026525.

Xie, J., Zhou, L., Zou, Z., Wang, J., Li, X., Chen, J., 2014. Continuously tunable reflective-type optical delay lines using microring resonators. Opt. Express 22 (1), 817. https://doi.org/10.1364/OE.22.000817.

Huang, M., Li, S., Xue, M., Zhao, L., Pan, S., 2018. Flat-top optical resonance in a single-ring resonator based on manipulation of fast- and slow-light effects. Opt. Express 26 (18), 23215. https://doi.org/10.1364/OE.26.023215.

Huang, M., Li, S., Yang, Z., Pan, S., 2019. Analysis of a flat-top optical ring resonator. Optics Commun. 451, 290–295.

Schwelb, O., 2005. Band-limited optical mirrors based on ring resonators: analysis and design. J. Lightwave Technol. 23 (11), 3931–3946.

J. Poon J. Scheuer S. Mookherjea G.T. Paloczi Y. Huang A. Yariv 12 1 90 10.1364/OPEX.12.000090.

Li, Q., Feng, Y., Wang, Z., Tang, X., Wang, X., 2013. Time delay with active single-ring and double-ring microresonator. Opt. Commun. 303, 67–72.

Chrostowski, L., Hochberg, M., 2015. Silicon Photonics Design: From Devices to Systems. Cambridge University Press, London.

H. Uetsuka, "AWG technologies for dense WDM applications," in IEEE Journal of Selected Topics in Quantum Electronics, vol. 10, no. 2, pp. 393-402, March-April 2004.

Manganelli, C.L., Pintus, P., Gambini, F., Fowler, D., Fournier, M., Faralli, S., Kopp, C., Oton, C.J., 2017. Large-FSR thermally tunable double-ring filters for WDM applications in silicon photonics. IEEE Photon. J. 9 (1), 1–10.

Inoue, K., Kominato, T., Toba, H., 1991. Tunable gain equalization using a Mach-Zehnder optical filter in multistage fiber amplifiers. IEEE Photon. Technol. Lett. 3 (8), 718–720.

Chryssou, C.E., 2000. Gain-equalizing filters for wavelength division multiplexing optical communication systems: a comparison of notch and long-period grating filters for integrated optoelectronics. Opt. Commun. 184 (5-6), 375–384.

Lenz, G., Madsen, C.K., 1999. General optical all-pass filter structures for dispersion control in WDM systems. J. Lightw. Technol. 17 (7), 1248–1254.

Zheng, P., Hong, H., Li, J., Hu, G., Yun, B., Cui, Y., 2019. Performances of microwave photonic notch filter based on microring resonator with dual-drive modulator. IEEE Photon. J. 11 (1), 1–13.

Y. Liu, D. Marpaung, A. Choudhary and B. J. Eggleton, "Highly selective and reconfigurable Si3N4 RF photonic notch filter with negligible RF losses," 2017 Conference on Lasers and Electro-Optics (CLEO), , pp. 1-2, San Jose, CA, 2017.

Liu, Y., Hotten, J., Choudhary, A., Eggleton, B.J., Marpaung, D., 2017. All-optimized integrated RF photonic notch filter. Opt. Lett. 42 (22), 4631. https://doi.org/10.1364/OL.42.004631.

A. Godbole, P. P. Dali, V. Janyani, T. Tanabe and G. Singh, "All Optical Scalable Logic Gates Using Si3N4 Microring Resonators," in IEEE Journal of Selected Topics in Quantum Electronics, vol. 22, no. 6, pp. 326-333, Nov.-Dec. 2016.

Chen, Q., Zhang, F., Zhang, L., Tian, Y., Zhou, P., Ding, J., Yang, L., 2014. 1 Gbps directed optical decoder based on two cascaded microring resonators. Opt. Lett. 39, 4255–4258.

S. Pan, Z. Tang, M. Huang and S. Li, "Reflective-Type Microring Resonator for On-Chip Reconfigurable Microwave Photonic Systems," in IEEE Journal of Selected Topics in Quantum Electronics, vol. 26, no. 5, pp. 1-12, Sept.-Oct. 2020.

A. Meijerink C.G.H. Roeloffzen R. Meijerink Leimeng Zhuang D.A.I. Marpaung M.J. Bentum M. Burla J. Verpoorte P. Jorna A. Hulzinga W. van Etten 28 1 2010 3 18.

G. Choo, C. K. Madsen, S. Palermo and K. Entesari, "Automatic Monitor-Based Tuning of an RF Silicon Photonic 1X4 Asymmetric Binary Tree True-Time-Delay Beamforming Network," in Journal of Lightwave Technology, vol. 36, no. 22, pp. 5263-5275, 15 Nov.15, 2018.

L. Zhuang et al., "Novel Ring Resonator-Based Integrated Photonic Beamformer for Broadband Phased Array Receive Antennas—Part II: Experimental Prototype," in Journal of Lightwave Technology, vol. 28, no. 1, pp. 19-31, Jan.1, 2010.

M. Burla et al., "Multiwavelength-Integrated Optical Beamformer Based on Wavelength Division Multiplexing for 2-D Phased Array Antennas," in Journal of Lightwave Technology, vol. 32, no. 20, pp. 3509-3520, 15 Oct.15, 2014.

B. Ortega, J. Mora and R. Chulia, "Optical Beamformer for 2-D Phased Array Antenna with Subarray Partitioning Capability," in IEEE Photonics Journal, vol. 8, no. 3, pp. 1-9, June.